Title:

Influence of the Reinforcement Distribution and Interface on the Electronic Transport Properties of MWCNT-Reinforced Metal Matrix Composites

Authors:

Sebastián Suarez, Nicolás Souza, Federico Lasserre, Frank Mücklich

This is the peer reviewed version of the following article:

Suarez, S., Souza, N., Lasserre, F. and Mücklich, F. (2016), Influence of the Reinforcement Distribution and Interface on the Electronic Transport Properties of MWCNT-Reinforced Metal Matrix Composites. Adv. Eng. Mater., 18: 1626-1633. DOI:10.1002/adem.201600216,

which has been published in final form at https://doi.org/10.1002/adem.201600216 .This article may be used for non-commercial purposes in accordance with Wiley Terms and Conditions for Use of Self- Archived Versions.

Influence of the reinforcement distribution and interface on the electronic transport properties of MWCNT-reinforced metal matrix composites

By *Sebastián Suarez*, Nicolás Souza, Federico Lasserre* and *Frank Mücklich*

[*] *Dr.-Ing. S. Suarez Corresponding-Author, Dipl.-Ing. N. Souza, M. Sc. F. Lasserre, Prof. Dr. F. Mücklich*
Functional Materials, Dept. of Materials Science and Engineering
Saarland University, Campus D 3.3, Saarbrücken, 66123. Germany.
E-mail: s.suarez@mx.uni-saarland.de

[**] *All authors wish to acknowledge the EFRE Funds of the European Commission for support of activities within the AME-Lab project. This work was supported by the CREATE-Network Project, Horizon 2020 Program of the European Commission (RISE Project N° 644013).*

Abstract

The transition towards an electricity-driven world is testing electrical contact materials to their limits. Specifically, new alternatives are needed where composites that sacrificed conductivity in exchange for reduced weldability and higher heat dissipation sufficed. Carbon nanotubes (CNT) have the potential to close the gap as ideal fillers due to their outstanding intrinsic properties, pushing the application limits further. However, the reported electrical conductivity measurements showed no clear tendency. In the present study we attempt to shed some light on this matter by focusing on the causes behind those results. We observed that the addition of 1 wt. % CNT improves the conductivity of nickel, followed by a drop for higher concentrations, measured by 4-point probe testing. Six nanotube orientation models describing different CNT arrangements were contrasted to the experimental data. Corrected values for nickel and CNT resistivities effectively place that of the composites close to the models, providing indications of a preferential orientation. We conclude that, in contrast to what is widely reported, the main contributing factors to the resistivity are inter-tube coupling, porosity and interfacial scattering, whereas clustering marginally influences the behaviour.

1. Introduction

Improving certain electrical characteristics in metals often results in other detrimental decay. Particularly in electrical contact materials, composites are not primarily intended to improve these properties, but to overcome other issues related to component duty life. For example, in low-voltage relays, Ag-based composites reinforced with ceramic particles are currently employed to avoid contact inter-welding and to increase the arc dissipation rate. These trade-offs outweigh the deterioration of other physical properties [1]. With the increasing tendency towards energy-efficient and reduced-weight materials, the search for a new type of functional reinforcement becomes mandatory. Carbon nanotubes (CNT) possess outstanding intrinsic physical properties, many of which surpass other common fillers in electrical contacts: e.g. outstanding thermal (up to 4000 K) [2] and chemical stability (low reactivity) [3], high thermal conductivity [4] and current carrying capacity [5]. Regarding the electrical properties, metal-CNT and CNT-CNT interactions are still unclear in the scientific community. Dissimilar reports regarding the electrical coupling of CNTs can be found, including several different governing effects. Due to their low dimensionality, it is predicted that the conductivity in CNTs (both, thermal and electrical) are ruled by quantum effects [6], whereas quasi-ballistic or diffusive mechanisms can be inferred from certain experimental investigations.

The electrical properties in metal/CNT composites are understudied in literature, providing limited information to build upon. Xu et al. found that for different CNT weight fractions (1, 4 and 10 wt.%), the electrical resistivity in CNT/Al composites showed increments of 44.1%, 94.1% and 61.7% respectively [7]. The authors state that CNT agglomeration at grain boundaries as well as carbide formation (AlC_2) increase electron scattering. In an attempt to improve CNT dispersion and interfacial contacts in an Al matrix, Nie et al. coated the nanotubes with molybdenum [8]. According to the authors, this did not improve the electrical conductivity of the composites due to low CNT and Mo

conductivities (compared to Al) and most probably, due to porosity (up to 5%). In electroless-deposited spark-plasma-sintered (SPS) MWCNT/Cu composites, the increase in the electrical resistivity was significant [9]. With MWCNT volume fractions ranging from 10 to 40 vol.%, the electrical resistivity reached up to 700% of the reference value for pure Cu. Again, the justification is based on the agglomeration of the CNTs on grain boundaries forming an interfacial phase, which is detrimental to the electron transfer. In the case of MWCNT/Ag composites produced by powder metallurgy, the electrical resistivity was increased up to 4.5 times that of pure Ag [10]. For concentrations above 10 vol.%, the increased amount of CNT/metal interfaces coupled with a large amount of porosity (from 12 to 24%) are both deemed unfavourable and held responsible for the decay in conductivity. However, Uddin et al. justified the improved electrical conductivity in SWCNT/bronze and MWCNT/bronze composites with the grain boundary distribution of CNTs [11]. They measured a 16.1 % improvement for very low CNT concentrations (0.1 wt.%), yet were unable to improve Cu matrix composites even up to 2 wt.% CNT. Finally, Yamanaka et al. [12] measured an increased conductivity in MWCNT/Ni with low concentrations (1 to 5 vol.%). These results are summarised in Table 1.

The present study attempts to explain the discrepancy observed within the published results by studying the mechanism acting in the electronic transport of MWCNT-reinforced metal matrix composites. For that MWCNTs were selected as the reinforcing phase due to the statistical fact that they possess at least one zero-gap layer [13], as opposed to SWCNTs which may be metallic or semiconducting. Thereby, certain unwanted effects can be avoided, such as Schottky barriers (formed at the metal-semiconductor junctions). Also, adjacent MWCNT walls are generally non-commensurate (possessing different chirality) with a negligible interlayer electronic coupling and could alternate between metallic and semiconducting [14]. The interlayer coupling in MWCNTs is comparable to graphite (approx. 10 meV) and is inversely proportional to the tube diameter [14]. This interlayer

coupling can be overcome by the available thermal energy at room temperature (300 K), which exceeds the aforementioned energy gap (k_B.T = 25.8 meV). Another report confirms that the charge transport between outer- and innermost layers is believed to be a tunnel transport [15]. However, several resistance-generating effects are unavoidable in composite processing, where interfaces determine the behaviour (such as Coulomb blockades, resonant tunnelling, Fano resonances, etc). The electrical resistance at interfaces becomes then of paramount importance, since both the matrix and the reinforcement are good electrical conductors. Therefore, a seamless and coupled integration would ideally improve the electron transfer to and from the reinforcement, efficiently reducing the energy losses in the applications.

The electrical properties were studied in bulk composites containing 1, 2 and 3 wt.% CNTs, manufactured by colloidal mixing in ethylene glycol and hot uniaxial pressing. The electrical resistivity was determined by means of a 4-point probe setup with scanning voltages from 1.0 to 3.0 V DC. The MWCNT cluster distribution of the 1 wt.% sample was evaluated with FIB/SEM tomography and the quantitative data of the reconstructed volume was analysed with a commercial software (MAVI). The experimental values of the resistivity were contrasted with established models in order to assess the arrangement of the CNTs within the composite.

2. Experimental

The starting materials are MWCNTs, commercially available as Baytubes C150P (purity >95 %, outer diameter distribution 5-20 nm, agglomerate size 0.1-1 mm), and dendritic Ni powder (Alfa Aesar, mesh -325). A colloidal mixing process was used to blend the precursor powders and is reported elsewhere [16]. The MWCNT/Ni ratios were 1, 2, and 3 wt.% (6.5, 12.3 and 17.5 vol.%, respectively, considering a MWCNT density of 1.3 $g.cm^{-3}$). Finally, the solvent was evaporated in a ventilated furnace. The dried powders were subsequently cold pressed under 990 MPa in cylindrical (diameter: 8 mm) steel dies to obtain green pellets. The pellets were sintered in a hot uniaxial press under vacuum (2 x 10^{-6} mbar) at 750 °C for 2.5 h with a 264 MPa axial pressure between Al_2O_3 pistons in graphite dies.

All sample densities were measured by the water buoyancy method, being over 98% of that predicted by the rule of mixtures.

The samples were characterised by field emission scanning electron microscopy (FE-SEM) using a Helios NanoLabTM 600 dual beam microscope (FEI Company) working at 5 keV and 0.69 nA. The interface between the Ni matrix and MWCNTs was evaluated by high-resolution transmission electron microscopy (HRTEM) on a Philips CM 200 working at 200 kV bias.

The electrical resistivity was determined by the 4-point probe method. The experimental setup (**Fig. 1**) consisted of a constant voltage source (Konstanter SSP 3000-52, Gossen Metrawatt), providing 1.0 to 3.0 V DC at room temperature (A to B), a multimetre (Keithley 2000) for the averaged (100 points) sample voltage drops (between C & D), and an oscilloscope (LeCroy Waverunner 6100A; 1 GHz) with a current probe (LeCroy CP031). The electrical resistance is obtained from the V-I curves and the specific resistivity ensues. It is worth noting that the full transversal cross-section was used to calculate the resistivity. This implies homogeneous electron transport throughout said cross-section between entrance and exit points.

3. Results and discussion

The mean values of the electrical resistivity and their corresponding standard deviations are shown in Table 2. A marginal improvement is observed for the 1 wt.% sample, with 3.3% lower resistivity than the reference. Yet, it lays within the values measured for pure Ni. However, for the rest of the sample set, very fluctuant values are observed. The 2 wt.% presents a resistivity significantly larger than the experimental Ni reference, whereas the 3 wt.% only shows a marginal increase of 4.2 %. The standard deviations of the 1, 2 and 3 wt.% samples reach below the experimental and the theoretical Ni, yet this only attests to the heterogeneity of the sample stack.

The electrical properties of Ni are not significantly affected up to large concentrations (3 wt.%), this corresponds to the empirical limit found in mechanical studies [17]. In comparison to the values reported in the literature (see Table 1), these results lay below what is generally reported. It can thus be

stated that the addition of CNTs does not affect the electrical resistivity under our experimental conditions. As mentioned before, this task is not trivial when attempting to improve the electrical properties of a metal.

Focusing on the sample which showed a marginal improvement (1 wt.%), a complementary analysis was performed by FIB/SEM tomography so as to quantify the connectivity between the clusters and electronic conduction through the network (**Fig. 2**). The reconstructed cluster distribution tends qualitatively towards a random distribution. Due to resolution and reconstruction limitations in FIB/SEM tomography, only clusters can be segmented and shown; their composition (CNT morphology, amount and orientation) remains unresolved.

The mathematical analysis (Table 3) of the CNT network was focused on two parameters, relevant for electrical and thermal properties, namely; the Euler number and the geometrical tortuosity. The Euler number represents the interconnectivity between particles, and the geometrical tortuosity shows the minimal path an electron would take from one extreme to the other. In our case the Euler number has a strong negative value, representing a strongly interconnected network [18]. This assertion is supported by a mean geometric tortuosity value close to one. The combination of these features leads to the assumption, that when an electron is injected into the CNT network, the strong interconnectivity would ensure its movement throughout the system. The only remaining hindering factors to the electron mobility in the system would therefore be inter-tube coupling and internal scattering.

As already mentioned, the tomography can show the connectivity of the clusters but cannot resolve whether the CNTs are aligned or not within each cluster. Thus, it would be necessary to assess this by alternative means.

The modelling of the electrical resistivity under different CNT arrangements and concentrations would serve as a reference and, upon comparison with experimental results, give an indication as to the most likely CNT orientation. Inversely, this allows to interpret the effect of CNTs on the electrical

properties of the composites. This approach has already been explored for other types of systems such as polymer/carbon composites [19]. The electrical resistivity was thus predicted as a function of CNT content with different arrangements (relative CNT and electrical current orientation) using diverse established models. These six models, summarised in Table 4, are those valid for conductivity/resistivity modelling, among many others with different applications. In the model equations, ρ_{eff} is the composite's effective resistivity, ρ_{matrix} the matrix resistivity, ρ_{CNT} the CNT resistivity and ϕ is the CNT volume fraction. The Rule of mixtures (ROM) is perhaps the most widespread method to model the physical properties of a composite material [20]. Particularly, the perpendicular (Reuss) and parallel (Voigt) (Table 4 - Eqs. 1 & 2) fibre orientation models (with respect to the current), are very useful as an initial approximation by defining upper and lower limits of conductivity for the behaviour of the composite.

These simplified models represent absolute maximum/minimum values for a highly anisotropic system. However, it is of interest to apply models which refine these boundaries by considering an isotropic and homogeneous composite in a large scale. For this case, the most suitable approach is that proposed by the Hashim-Shtrikman (H-S) model, represented in equations 3 and 4 (Table 4)[21]. Both upper (H-S_u) and lower (H-S_l) bounds of the effective property of the composite modelled by H-S will lay within the previously defined ROM bounds [21].

On the other hand, said boundary models consider a perfect reinforcement distribution throughout the matrix. If the random nature of the process is considered, an arbitrary distribution must be taken into account. In the case of this study, two approaches were made in this sense. The first one consists in the application of an EMT (effective medium theory) model [20], which deals with a random distribution of reinforcements (Table 4 - Eq. 5). This is a general expression which under certain conditions (particles distant from each other, so as to avoid local distortions) leads to the well-known

Maxwell-Garnett model. However, it has been demonstrated that this model also fits the case where particles are in close proximity to each other [22].

Additionally, a model proposed by Hamilton (HAM) —which takes into account the shape of the reinforcement— was also adjusted to the studied concentrations, and is described by equation 6 (Table 4)[23]. This model focuses on the study of the influence of non-spherical particles by introducing the shape factor *n* into the equation (n=6 for cylindrical inclusions). The term α represents the resistivity ratio as $\alpha = \rho_{CNT}/\rho_{matrix}$.

Initially, the theoretical resistivity for Ni (6.99×10^{-8} Ω.m) [24] and that of CNTs provided by Hjortstam et al. (0.35×10^{-8} Ω.m) [25] were considered. In this evaluation, a large deviation between the experimental data and the proposed models is observed (**Fig. 3a**: pink hatched surface). The value of the pure sintered Ni sample deviates significantly from the theoretical value. This is expected, since the theoretical value corresponds to highly pure, defect-free Ni. In spite of full density, our sintered Ni may present a certain amount of internal oxidation as well as a considerable amount of defects, which were not quantified in this study. Therefore, for a more realistic approximation, the experimental value for our pure Ni samples (8.05×10^{-8} Ω.m) was utilised in a second iteration of the modelling (**Fig. 3a**: bottom half curves). The new curves still deviate from the composites, yet the Voigt, HAM, H-S (lower bound) and EMT models approach the averages and intersect the dispersions.

These approximations still do not fit the experimental results, possibly due to the resistivity value of the CNTs which is still under scrutiny in the community. This rather optimistic value is even below highly conductive metals such as Ag (1.58×10^{-8} Ω.m), Cu (1.68×10^{-8} Ω.m) and Al (2.65×10^{-8} Ω.m) [24] and two orders of magnitude lower than in-plane highly ordered pyrolytic graphite (HOPG, ca. 4×10^{-7} Ω.m) [24]. Ebbesen et al. reported more conservative values obtained experimentally [26]. Therefore, a mean of said values (2.8×10^{-6} Ω.m), in decent correlation with other reported values for MWCNTs, was considered for a third iteration (**Fig. 3b**: top-half curves), with the experimental

resistivity for Ni maintained. In this case, the experimental data shows an acceptable correlation to the Voigt approximation. This correlates well with CNT-containing diametral planes (XZ of the sample), formed orthogonally to, and caused by, the pressing direction during fabrication (as per **Fig. 1**). The current and voltage drop measurements were made along these planes, meaning a parallel or in-plane current. This explanation also holds in a final, more realistic iteration, considering the filling phase as CNT agglomerates, rather than single tubes. The corresponding resistivity ($4.5x10^{-5}$ Ω.m) [27] results in an expanded range covered by the different models, as shown in **Fig. 3b**. All samples are thus closer to an in-plane random arrangement fitted with the Voigt distribution model.

If we focus on the samples that showed a mean resistivity higher than the Ni reference (2 and 3 wt.%), this increase could be explained due to a reduced wettability of agglomerates to the metallic matrix, as seen in previous investigations [17][28]. Agglomerate size in higher CNT concentrations tend to be larger, thus reducing the real contact area between matrix and reinforcements [29]. This would severely hinder the electron injection to the CNT network and thus, the CNT-filled voids would effectively act as plain porosity. A good dispersion must translate to a homogeneous distribution and an enhancement of the matrix properties facilitating the electrical and thermal transport through the interface.

The applied models are quite limited and severely underpredict the influence of the interfaces and agglomeration of the CNTs. After extensive literature research, it was not possible to find a proper model that would adequately consider these neglected features. Furthermore, the actual values of the interfacial resistance between metals and CNTs are still a topic of discussion within the community. A review study on this topic classifies the contact resistance between MWCNTs and metals into two categories: side and end contacts [30]. The former ranges from 1.7 to 50 kΩ and the latter from 50 to 300 kΩ. A clear conclusion that can be drawn from these values is that electrons in CNT/metal composites would preferentially flow through end-contacts instead of side-contacts. The resistance in

side-contacts may generate a tunnelling barrier with a Coulomb blockade [31]. However, it is expected that in this type of composites, the interfacial area between CNTs and metals is sufficiently large so as to shift the resistance towards the lowest values [30][31]. For this system, a seamless interface was observed by high resolution TEM (**Fig. 4**). The main interfacial connection between the agglomerate and the matrix seems to be a side-contact type, however end-contacts cannot be dismissed.

In the case of an optimal coherent contact of MWCNTs in Au/Ti (full coating of the CNT with metal), the contact resistance is expected to decrease with a greater number of contacted layers/shells (532 Ω for 24 contacted shells and 480 Ω for 27) [32]. To achieve this, an intimate contact at the open end of each MWCNT would have to be generated, therefore obtaining a multiple contact of all concentric walls.

Concerning the MWCNT agglomerates, the literature provides very interesting information that was somehow disregarded in the previous studies in metal/CNT composites. As shown before, all the reports base their discussion on the negative effect that the agglomerates have on the electrical conduction. Remarkably, the electrical properties of agglomerates are not as low as to generate such a decrease in the conductivity. For example, Aliev et al. show curves of MWCNT sheets measured in different directions, and their values are still acceptable compared to those of semiconductive or ceramic reinforcements [33]. Even when the MCWNTs are subjected to highly energetic processing (such as SPS), they tend to form a percolation path through the network with resistivities as low as 10^{-5} Ω.m [27][34].

Contact between CNTs is believed to be governed by quantum resonant effects such as resonant tunnelling or the Fano effect. For a better understanding of these effects, the system can be equivalently represented as the electronic coupling between a quantum wire and a quantum dot. An electron travelling through the quantum wire can be at a certain moment coupled to an electron within the dot, exciting it and inducing its movement in another direction. This local coupling and consequent

(diffusive) energy loss, although detrimental to the conduction of the initial electron, is responsible for the overall conduction in the composite. Furthermore, Santini et al. found that the contact resistance in a MWCNT/MWCNT contact was always below the MWCNT/metal contact resistance for all the different nanotube diameters tested, therefore showing great potential to be used as horizontal interconnects [35]. The transfer mechanisms involved in the process at the interface are still a topic of discussion within the community. There are approaches in which a single CNT is contacted by metal oxides at either end, building a transistor. In these studies, it was very difficult to analyse the interfacial transport, reporting an absolute interfacial resistance which is strongly influenced by numerous factors [36]. An issue that is still left to prove is the formation of Schottky barriers in the contact when a graphene semiconducting layer is met by the electron. Theoretically, Schottky barriers would not be an issue, since the barrier formed between a metal and a semiconducting CNT layer has a width of a few nanometres and electrons can tunnel through it [31].

Summarising, it can be observed that in the study of the electrical behaviour of metal/CNT composites, the participation of CNT agglomerates in the decrease of the conductivity is usually overestimated. The literature provides very useful information that would indicate that the main factor ruling the decay in the conductivity would be the detachment of the CNTs (individual tubes or agglomerates) from the matrix. This effect would be seen (from an electrical perspective) as porosity, and therefore as a detrimental factor. As shown in **Fig. 5**, the increase in the CNT concentration leads to a decrease in interfacial contact with the matrix. When working with voltages over a certain threshold (in the mV-V range) coupled with a proper manufacturing technique (high final densities), all the unfavourable effects such as interfacial resistance, inter-tube tunnelling resistance (above 1.8 nm separation) [37], interlayer isolation and energy gaps can be straightforwardly overcome, resulting in some cases, in an improved electrical conduction.

4. Conclusions

By placing our experimental results within the context of the available literature, this study attempts to identify the actual causes related to the increase in the electrical conductivity of metal/CNT composites. Contrary to what is reported in the literature, MWCNT agglomeration is, at least directly, not the main factor in the conductivity loss, being greatly outweighed by their cohesion to the matrix. This is observed particularly in higher CNT concentrations, where the MWCNTs do not show a proper contact to the matrix.

The comparison to established models was useful to interpret the reinforcement distribution (i.e. the MWCNTs) and alignment with respect to the electrical current, and to establish the shortcomings of said models in order to advance subject. As expected, the MWCNT networks in the 1, 2 and 3 wt.% samples are aligned in planes, perpendicular to the pressing axis from the fabrication. These planes are collinear to the current applied for the electrical measurements. In the largest evaluated concentration, the most suitable model describes a totally random distribution, which could be correlated to unordered agglomerates.

A quantitative analysis of the CNT clusters showed a strong interconnectivity and a straightforward path for the electrical current. Furthermore, it was observed that in lower CNT concentrations, a seamless interface is present, implying predominantly side CNT contacts. The presented results might be useful as a first assessment for the design of composites for electrical (contact materials) or electronic (packaging materials) applications.

References

[1] N. Jeanvoine, a. Velichko, C. Selzner, F. Mücklich, *Eur. Phys. J. Appl. Phys.* **2009**, *49*, 22907.

[2] H. Pierson, *Handbook of Carbon, Graphite, Diamond and Fullerenes*, Noyes Publications, Park Ridge, NJ **1993**.

[3] J.Y. Hwang, a. Neira, T.W. Scharf, J. Tiley, R. Banerjee, *Scr. Mater.* **2008**, *59*, 487.

[4] S. Berber, Y. Kwon, D. Tomanek, *Phys. Rev. Lett.* **2000**, *84*, 4613.

[5] B.Q. Wei, R. Vajtai, P.M. Ajayan, *Appl. Phys. Lett.* **2001**, *79*, 1172.

[6] C. Dekker, *Phys. Today* **1999**, 22.

[7] C. Xu, B. Wei, R. Ma, J. Liang, X. Ma, *Carbon N. Y.* **1999**, *37*, 855.

[8] J. Nie, C. Jia, N. Shi, Y. Zhang, Y. Li, X. Jia, *Int. J. Miner. Metall. Mater.* **2011**, *18*, 695.

[9] W.M. Daoush, *Powder Metall. Met. Ceram.* **2009**, *47*, 531.

[10] Y. Feng, H.L. Yuan, M. Zhang, *Mater. Charact.* **2005**, *55*, 211.

[11] S.M. Uddin, T. Mahmud, C. Wolf, C. Glanz, I. Kolaric, C. Volkmer, H. Höller, U. Wienecke, S. Roth, H.-J. Fecht, *Compos. Sci. Technol.* **2010**, *70*, 2253.

[12] S. Yamanaka, R. Gonda, A. Kawasaki, H. Sakamoto, Y. Mekuchi, M. Kuno, T. Tsukada, *Mater. Trans.* **2007**, *48*, 2506.

[13] J. Robertson, G. Zhong, S. Hofmann, B.C. Bayer, C.S. Esconjauregui, H. Telg, C. Thomsen, *Diam. Relat. Mater.* **2009**, *18*, 957.

[14] P.R. Bandaru, *J. Nanosci. Nanotechnol.* **2007**, *7*, 1239.

[15] K. Tsukagoshi, E. Watanabe, I. Yagi, N. Yoneya, Y. Aoyagi, *New J. Phys.* **2004**, *6*, 3.

[16] S. Suarez, F. Soldera, C. González Oliver, D. Acevedo, F. Mücklich, *Adv. Eng. Mater.* **2012**, *14*, 499.

[17] S. Suarez, F. Lasserre, F. Mücklich, *Mater. Sci. Eng. A* **2013**, *587*, 381.

[18] J. Ohser, F. Mücklich, *Statistical Analysis of Microstructures in Materials Science*, John Wiley & Sons, Chichester (UK) **2000**.

[19] Z. Garncarek, R. Piasecki, J. Borecki, A. Maj, M. Sudol, *J. Phys. D. Appl. Phys.* **1996**, *29*, 1360.

[20] M. Wang, N. Pan, *Mater. Sci. Eng. R Reports* **2008**, *63*, 1.

[21] D. McLachlan, M. Blaszkiewicz, R. Newnham, *J. Am. Ceram. Soc.* **1990**, *73*, 2187.

[22] K. Yoshida, *Philos. Mag. B* **1986**, *53*, 55.

[23] R.. L. Hamilton, O.K. Crosser, *I EC Fundam.* **1959**, *1*, 187.

[24] D.R. Lide, *CRC Handbook of Chemistry and Physics*, CRC Press**2009**.

[25] O. Hjortstam, P. Isberg, S. Söderholm, H. Dai, *Appl. Phys. A Mater. Sci. Process.* **2004**, *78*, 1175.

[26] T. Ebbesen, H. Lezec, H. Hiura, J. Bennett, H. Ghaemi, T. Thio, *Nature* **1996**, *382*, 54.

[27] K. Yang, J. He, Z. Su, J.B. Reppert, M.J. Skove, T.M. Tritt, A.M. Rao, *Carbon N. Y.* **2010**, *48*, 756.

[28] S. Suárez, E. Ramos-Moore, F. Mücklich, *Carbon* **2013**, *51*, 404.

[29] P. Rossi, S. Suarez, F. Soldera, F. Mücklich, *Adv. Eng. Mater.* **2015**, *17*, 1017.

[30] Q. Ngo, D. Petranovic, S. Krishnan, *IEEE Trans. Nanotechnol.* **2004**, *3*, 311.

[31] F. Banhart, *Nanoscale* **2009**, *1*, 201.

[32] P.J. de Pablo, E. Graugnard, B. Walsh, R.P. Andres, S. Datta, R. Reifenberger, *Appl. Phys. Lett.* **1999**, *74*, 323.

[33] A.E. Aliev, C. Guthy, M. Zhang, S. Fang, A. A. Zakhidov, J.E. Fischer, R.H. Baughman, *Carbon* **2007**, *45*, 2880.

[34] J. Li, L. Wang, T. He, W. Jiang, *Carbon* **2009**, *47*, 1135.

[35] C. a. Santini, A. Volodin, C. Van Haesendonck, S. De Gendt, G. Groeseneken, P.M. Vereecken, *Carbon* **2011**, *49*, 4004.

[36] B. Corso, I. Perez, P. Collins, *ECS Trans.* **2012**, *41*, 27.

[37] C. Li, E.T. Thostenson, T.-W. Chou, *Appl. Phys. Lett.* **2007**, *91*, 223114.

List of Figures

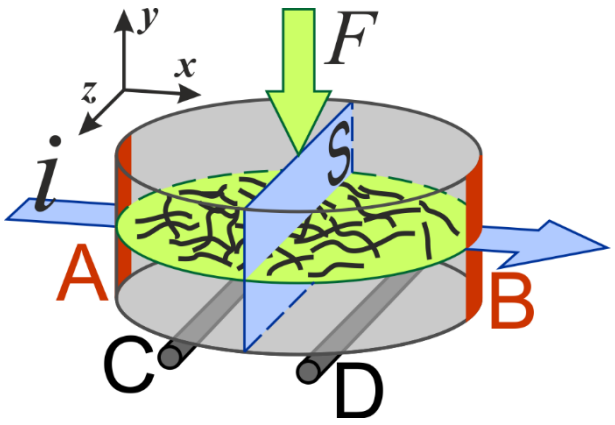

Fig. 1. Diagramme of a composite pellet with the current measured diametrically (AB), supposed travelling through the full cross-section (S), with a voltage drop measured between the wires (C & D). The pressing direction (F) is thought to orient the CNTs in XZ planes.

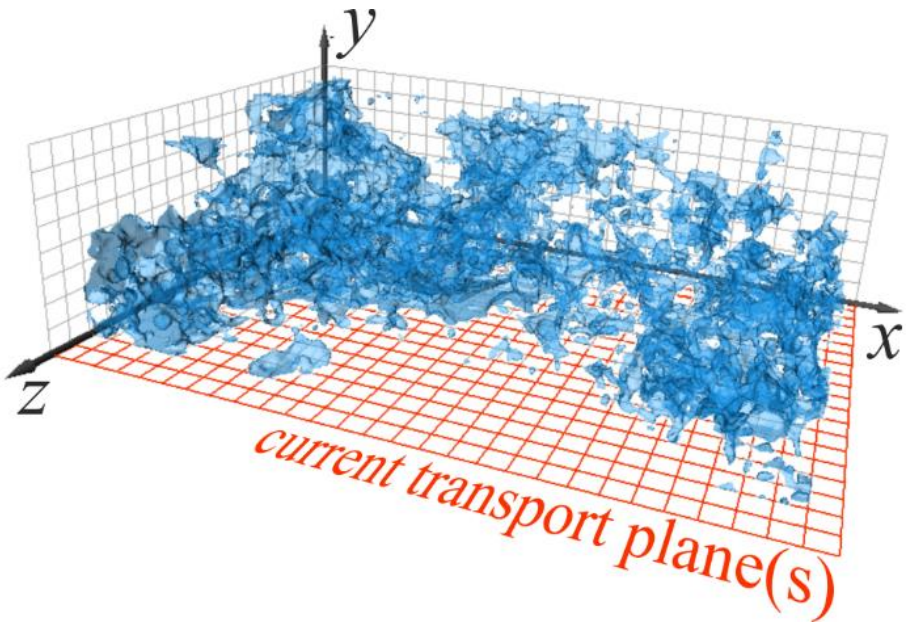

Fig. 2. FIB/SEM tomography of the CNT cluster distribution in a MWCNT/Ni 1 wt.% composite. The interconnectivity between the clusters is thus clearly depicted. The analysed volume is 28x8x18 µm3. The XZ planes contain the measured conduction paths.

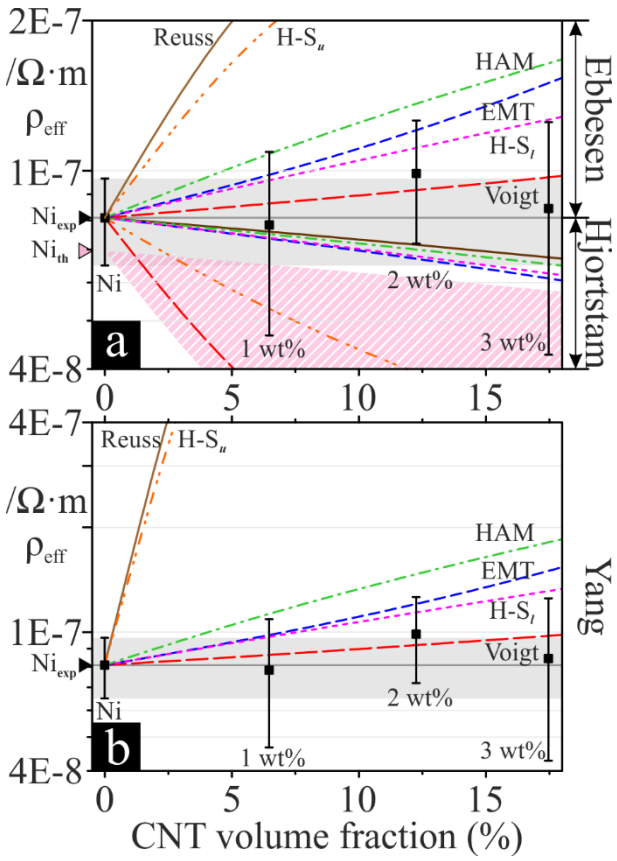

Fig. 3. Experimental resistivities for Ni and Ni/CNT composites versus CNT fraction, including that of predicted composite models. Four modelling iterations incorporating different values for CNTs and Ni, respectively, from: (a: pink hatched surface, i.e., range covered by all models) Hjortstam + theoretical Ni, (a: bottom half) Hjortstam + experimental Ni, (a: top half) Ebbesen + experimental Ni and (b) Yang + experimental Ni.

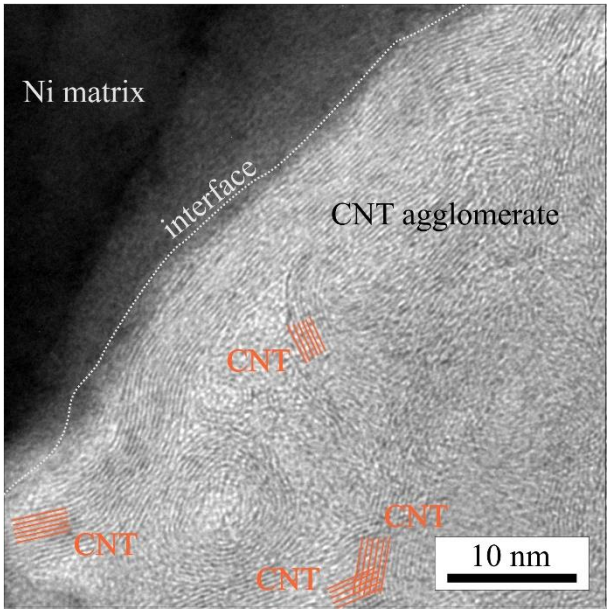

Fig. 4. HR-TEM micrograph of the interface between a CNT agglomerate and the Ni matrix in a 1 wt.% composite. In orange, different CNTs within the agglomerate are highlighted.

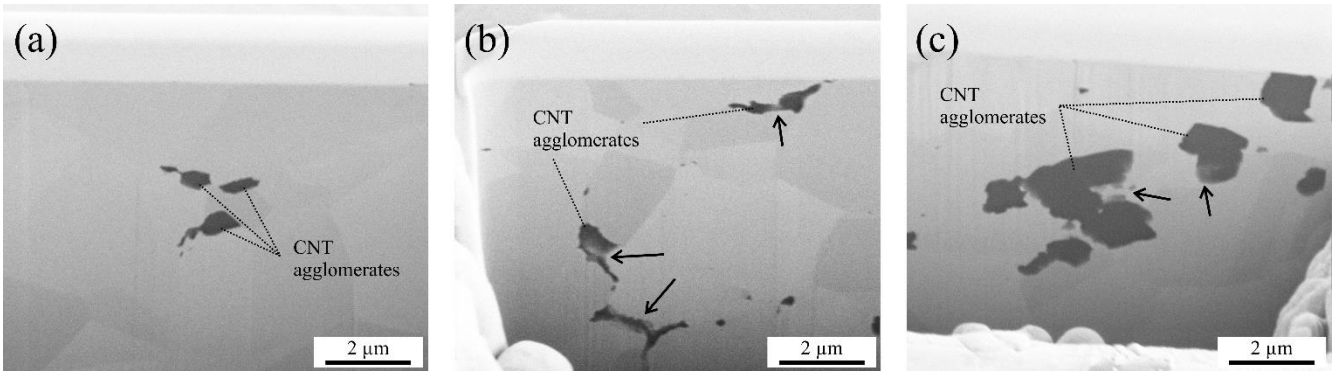

Fig. 5. FIB/SEM cross-section of the studied composites. (a) 1 wt.% CNT, (b) 2 wt.% CNT and (c) 3 wt.% CNT. The dashed lines indicate the position of the CNT agglomerates. The arrows indicate the places where the agglomerates lose the interface with the matrix.

List of tables

Table 1. Summary of the reported resistivity in CNT-reinforced Metal Matrix Composites. The best results per study are in bold and improvements are highlighted in grey.

Matrix	Filler	Fabrication	CNT fraction [wt.%]	Relative resistivity [%]	Explanation	Reference
Al	CNT	Hand grinding + pressing @ 25 MPa (793 K, 30 min)	1	**44.1**	Agglomeration and carbide formation	Xu et al. [7]
			4	94.1		
			10	61.8		
Al	Mo coated CNT	Stirring or Mechanical milling + Grinding + SPS @40MPa (580°C, 5 min)	0.25	**6.3**	Low CNT and Mo conductivities; Porosity	Nie et al. [8]
			0.5	**6.3**		
			1	9.4		
			2	12.5		
Ag	MWCNT	Hand grinding + Press@320MPa (2min) + Sintered @700°C + Press @400MPa	~4	**18.8**	Increased amount of CNT/Ag interfaces; Porosity	Feng et al. [10]
			~9	25.0		
			~13	50.0		
			~19	256.3		
			25	500.0		
Cu	CNT	Electroless coating of CNT + SPS @20MPa (600°C, 1 min)	10	**345.0**	Filler/matrix conductivity disparity and grain boundary CNT agglomerates	Daoush [9]
			20	440.0		
			30	565.0		
			40	675.0		
Cu	MWCNT	Ball milling + Hot Press sintering @ 40 MPa (750 °C)	0.1	**17.7**	Porosity	Uddin et al. [11]
			0.5	23.5		
			2	294.0		
Bronze	SWCNT	Ball milling + Hot Press sintering @ 40 MPa (800 °C)	0.1	**-16.1**	CNTs at grain boundaries	
			0.5	-1.6		
Bronze	MWCNT		0.1	-9.4		
			0.5	-3.6		
Ni	MWCNT	Slurry mixing+SPS@ 50 MPa (673-1073K)	1 vol.%	0.0	Ballistic effect in MWCNT	Yamanaka et al. [12]
			2 vol.%	-1.2		
			3 vol.%	**-2.5**		
			4 vol.%	2.5		
			5 vol.%	-1.2		
			10 vol.%	13.3		

Table 2. Experimental values of the electrical resistivity of the composites with different CNT concentrations. Improvement is highlighted in grey

CNT [wt.%]	CNT [vol.%]	Electrical resistivity [x10^{-8} Ω.m]	Relative resistivity [%]
Pure Ni	-	8.05 ± 1.60	---
1.0	6.5	7.79 ± 3.12	-3.3
2.0	12.3	9.87 ± 2.73	22.6
3.0	17.5	8.39 ± 4.12	4.2

Table 3. Field parameters for a MWCNT/Ni 1 wt.% composite, reconstructed after a FIB/SEM tomography.

Direction	Mean geometric tortuosity	Max. geometric tortuosity	Min. geometric tortuosity	Euler number
X	1.00664	1.02469	1	
Y	1.01507	1.11178	1	− 874
Z	1.02652	1.21429	1	

Table 4. Summary of the different models used to describe the distribution of two phases for conductivity / resistivity.

Model	Distribution	Case / Particularity	Formula	Eq.
ROM	anisotropic	Reuss (perpendicular)	$\rho_{eff} = (1-\phi)\cdot\rho_{matrix} + \phi\cdot\rho_{CNT}$	(1)
		Voigt (parallel)	$\rho_{eff} = \left[\frac{1-\phi}{\rho_{matrix}} + \frac{\phi}{\rho_{CNT}}\right]^{-1}$	(2)
H-S	isotropic	upper bound	$\rho_{upper} = \rho_{CNT} + \frac{1-\phi}{\frac{1}{(\rho_{matrix}-\rho_{CNT})} + \frac{\phi}{3\cdot\rho_{CNT}}}$	(3)
		lower bound	$\rho_{lower} = \rho_{matrix} + \frac{\phi}{\frac{1}{(\rho_{CNT}-\rho_{matrix})} + \frac{1-\phi}{3\cdot\rho_{matrix}}}$	(4)
EMT	random		$(1-\phi)\cdot\frac{(\rho_{matrix}-\rho_{eff})}{(\rho_{matrix}+2\cdot\rho_{eff})} + \phi\cdot\frac{(\rho_{CNT}-\rho_{eff})}{(\rho_{CNT}+2\cdot\rho_{eff})} = 0$	(5)
HAM		shape factor	$\frac{\rho_{eff}}{\rho_{matrix}} = \frac{\alpha+(n-1)+(n-1)\cdot(\alpha-1)\cdot\phi}{\alpha+(n-1)+(1-\alpha)\cdot\phi}$	(6)